Applied Mathematical Modelling 128 (2024) 450–469

Contents lists available at ScienceDirect

Applied Mathematical Modelling

journal homepage: www.elsevier.com/locate/apm

Forced vibration analysis of beams with frictional clamps

Mertol Tüfekci [a], John P. Dear [a,*], Loïc Salles [a,b]

[a] Imperial College London Department of Mechanical Engineering, Exhibition Road, London, SW7 2AZ, UK
[b] University of Liège, Department of Aerospace and Mechanical Engineering, Mechanical Aspects of Turbomachinery and Aerospace Propulsion, 4000 Liège, Belgium

ARTICLE INFO

Keywords:
Beam vibrations
Friction damping
Nonlinear force
Analytical solution
Frequency response

ABSTRACT

This study investigates the vibration characteristics of rectangular cross-sectioned and straight beams with imperfect supports, focusing on the role of dry friction at the contact interfaces. The contact interactions are reduced to resultant point loads, and the friction at the contact interfaces is modelled using the Jenkins friction model, introducing nonlinearity into the system. These nonlinear terms are included in solution-dependent boundary conditions for the governing differential equation of beam vibration. Two cases are considered in detail and solved: one where the beam is tightened between rigid clamps at both ends and excited from the middle with a harmonic displacement function, and another where only one end is clamped with the other end free but excited with an imposed harmonic displacement. The governing differential equation is solved analytically, separating the motion into two distinct regimes - full-stick and full-slip, using the Galerkin method. The results acquired from this analytical model are then compared to those from a numerical model, which is built and solved using the finite element method combined with a frequency sweep and time-marching.

1. Introduction

Beams are the simplest continuous mechanical structures that are representative of real-world applications. This simplicity makes their mechanical behaviour relatively easier to predict. Due to their predictable behaviour, they are one of the most commonly used objects for a wide spectrum of research that spans from applying/exploring different theories and performing experiments. Researchers use beams in many experimental studies to test and compare hypotheses and parameters like material properties [1]. Exploring mechanical behaviours through advanced analytical methods, such as the isogeometric approach to the free vibration analysis of Bernoulli–Euler and Rayleigh curved beams, has furthered our understanding of beam dynamics in complex scenarios [2]. The predictability of beams, especially uniform straight beams, roots from simple mathematical formulations for modelling their mechanics. The simplicity of their mathematical formulations makes it easier to develop analytical solutions [3,4]. A varying cross-section, of course, changes the governing equations and, consequently, the behaviour of the system whilst introducing complexities to the mathematical side of the problem [5]. Recent studies have expanded this understanding by incorporating advanced beam theories, such as the modified couple stress theory and the differential quadrature method, to capture size effects in microbeam vibration analysis [6,7].

* Corresponding author.
E-mail address: j.dear@imperial.ac.uk (J.P. Dear).

https://doi.org/10.1016/j.apm.2024.01.031
Received 11 October 2023; Received in revised form 3 January 2024; Accepted 22 January 2024

Available online 26 January 2024

Complexities do not have to arise from geometry alone; they can also stem from material behaviour. Due to their relatively simple formulations, beams are considered as good instruments to make consistent comparisons between material models [8–10]. For instance, the thermo-elastic vibrational behaviour of microbeams, studied under various conditions including size effects and thermal environments, has provided valuable insights into how external factors, such as temperature, influence beam vibration [11,12]. Composite materials represent one of the more complex cases. The theory of composites introduces additional material properties/parameters to the constitutive equations and, hence, indirectly to the beam equations [13]. Therefore, beams have also been employed as objects in the modelling of composites [14–17]. This is further illustrated by studies on the dynamic response of fibre-reinforced composite beams under various loading conditions, where approaches like the Timoshenko beam theory and the Ritz method have been utilised to analyse the kinematics of composite beams [18,19]. Moreover, the nonlinear dynamic response and buckling behaviour of functionally graded microbeams, incorporating geometric imperfections and analysed using a unified shear deformable beam theory, demonstrate the complexity introduced by varying material properties [20–22].

Apart from these, damping can be considered a concept that is as old as vibration [23]. Hence, it is one of the most important properties that is investigated in the literature [24,25]. However, damping is not fully a material property, it can root from other structural reasons as well as the material itself [26]. Its importance lies in the effect on the dynamic behaviour of the mechanical system [27].

In terms of material damping, there are various approaches to model the damping behaviour of materials [28–30]. Each approach fits better into different cases, mostly, it dominantly depends on the mechanical properties of different types of materials. The reason for the existence of different damping modelling techniques is the complex mechanisms of materials and structures that lead to damping [31–33]. These damping mechanisms are still not completely understood. To get a better understanding, beams are often employed by researchers to investigate damping models [34]. More specifically, beams are found successful in displaying the differences between different damping models [17,35]. The reason behind their success is their structural simplicity. The beams do not have as many parameters as plates/shells or any other continuous structures that affect the dynamics, and the existing parameters are relatively easy to control/restrict.

There are more sources of damping other than material damping, which can be called as external damping [36–38]. The external damping is usually modelled as external loads. One of the external sources of damping can be stated as the fluids in which the mechanical system is placed. Air is one of such fluids. The external aerodynamic forces can add damping to the mechanical system [39–41]. Furthermore, foundations with damping capabilities can also add terms to the external forces as well as the stiffness [42,43].

As one of the most common external damping, friction is to be found [44,45]. Friction is one of the areas that has been actively researched for centuries. The effects of friction are observed by humankind, and these effects are reduced by inventing the wheel and also are used to set fire [46]. The history of friction roots back to ancient Rome and ancient Greece. Themistius and Aristotle are among the people who had ideas about the friction concept. Themistius even differentiates the static and kinetic friction in the 4^{th} century [47]. Long before Themistius, it is known that ancient people benefited from the damping capabilities of friction. Friction helped the ancient people to reduce the destructive effects of vibrations (usually earthquakes) and to build greater structures with magnificent architecture [48]. A good example would be the Parthenon. Between the marble drums of the columns of the Parthenon, there are wooden pinned joints instead of using some kind of grout or soil mixture. This reduces the stiffness and adds frictional damping to the structure. As a result, the stresses occurring during earthquakes are significantly reduced [49,50]. Much later but still before the concepts of damping, friction and even force are formally and scientifically expressed, Leonardo da Vinci displays the effects of friction using sliding blocks [51]. Amontons, Leonard Euler and finally, Coulomb's works follow in the following decades and centuries [51–53]. As of today, the fields of contact and friction still attract enormous attention with a promising future with many unknowns yet to be discovered.

It is also crucial to stress that the effects of friction on mechanical systems are significant. Since the nature of friction is complicated and the effects are important, various methods are employed, including analytical, numerical and experimental techniques, to understand the mechanism and effects. Besides, friction is a very common phenomenon and usually is unavoidable, especially in multi-body systems [54]. From the example of the Parthenon, it can be confidently claimed that friction can be considered as a major factor that adds damping to the mechanical systems [55,56]. The contribution of friction to damping can be investigated in many different ways. As a consequence, there are various modelling techniques for friction itself [53,57,58]. Among these techniques, the expression of friction forces depending on slip velocity and/or displacement using functions such as Benson, Coulomb, and smooth Coulomb functions stand out in the literature [53,59–61].

Another important matter to point out is that friction leads to nonlinear behaviour, which brings additional difficulty in terms of solution. To handle the problem, the calculation of linear equivalence of such nonlinear systems, in other words, linearisation, helps up to some extent providing a solution with a limited range and level of accuracy [62,63]. Dealing with more complex models, that are still analytically solvable, increases the level of accuracy significantly [64–66]. As the industry developed, more complicated structures are needed to be built. Consequently, even more complex models are developed, and the complexity of those models reaches the point of being analytically solvable [67]. These different nonlinear models are solved by employing numerical methods such as harmonic balance, time marching and finite element method [68,69].

The time marching methods are a commonly used solution approach for nonlinear equilibrium equations, providing a higher degree of accuracy, although they sometimes are computational expensive, especially in the presence of friction nonlinearities [70]. The predictor/multi-corrector time marching with automatic adaptivity is one such approach that is noted for its stability and computational efficiency, and is used for solving hyperbolic partial differential equations in various domains [71]. Moreover, Burlayenko and Sadowski deal with the nonlinear dynamic responses of systems subjected to harmonic loading in time and frequency domains [72].

Even the most complicated nonlinear models use idealisations and simplification assumptions to make the governing equations solvable or at least computationally more reasonable. Therefore, imperfections, such as compliance of supports and friction at the contact interfaces of supports, are usually neglected [73–75]. But in some cases, these imperfections may cause significantly different mechanical behaviour than the idealised model [76]. Some of these imperfections are quite hard to predict because of the lack of insight into their governing actual mechanisms. These imperfections can be handled as uncertainties [77,78]. In order to conduct the modelling of such uncertainties, stochastic modelling is one of the most common techniques [79]. Focusing on supports for beam structures, there are works employing uncertainties to model complex boundary conditions [80,81].

As one of these imperfections, friction plays a crucial role since it may change the characteristics of a beam-clamp-support system significantly [82,74,83,75,69]. If not predicted accurately, this deviation caused by friction can lead to inappropriate designs. This can even cause unexpected failure in structural systems. This effect is most apparent in practical applications such as the design and analysis of mechanical test rigs or certain types of engineering structures. For instance, in experimental test rigs, such as those used in material damping measurements, friction can significantly influence the damping data. Unaccounted friction in these setups can lead to misleading results, which is the motivation behind this study. Similarly, frictional effects in structural components like turbine or compressor blades of aircraft engines, which can be modelled as cantilever beams, can impact their performance and lifespan. These components often operate under high-vibration environments, making the accurate modelling of frictional effects crucial for their design and analysis.

Hence, in this study, a new efficient technique/method is developed to model the dynamic flexural behaviour of Euler-Bernoulli beams with frictional supports conducting an analytical solution to the problem. Since the formulation uses Euler-Bernoulli beams with straight axes, it is assumed that axial, torsional and bending motions are decoupled. This model takes into account that friction can add damping to the system. In order to express the forces and moments at the supports, a Newtonian approach and to model friction, displacement-dependent formulations and modelling approaches are utilised. By drawing the free-body diagrams of the clamps and the beams, the interaction is analysed, and the effective reaction forces and moments are formulated. These effective reactions are plugged into the governing beam vibration equation as nonlinear external forces with relative slip dependence. The outcoming nonlinear partial differential equation is solved analytically. In order to validate the model, a finite element model is built and solved in the time domain for various excitation frequencies numerically. The results of both analytical and numerical models are compared. Finally, the effect of friction on the dynamic behaviour of beams is discussed over a numerical example and a parametric study. There is no study found in the literature that handles the frictional vibration of beam-clamp systems analytically using the Galerkin method separately for full-stick and full-slip regimes. This proves to be a computationally efficient and very accurate technique. Such beam-clamp systems can be representative of many real-life applications, such as fan/turbine blades of an aircraft with friction at their roots as well as vibration testing systems. Thus, this method is expected to be useful in the design processes of a variety of engineering applications.

2. Analysis and formulation

The formulation considers only the in-plane bending motion of a beam with a uniform rectangular cross-section. Assuming small displacements and the presence of simple bending motion, the typical equation of motion for bending of Euler-Bernoulli beams is used, and that is given as:

$$\rho A \frac{\partial^2 v}{\partial t^2} + EI \frac{\partial^4 v}{\partial z^4} = 0 \tag{1}$$

It is important to stress that no external load terms appear in this equation of motion since the excitation and friction are handled in the boundary conditions.

A beam with a cross-sectional area A, density ρ, elasticity modulus E and area moment of inertia I, that is excited with an imposed displacement from a point far away from the clamps in the transverse direction is modelled. Here, z is the axial coordinate that starts from the clamp and goes along the beam, t denotes the time, and v indicates the transverse deflection of the beam.

For this case, a free body diagram for a beam with frictional clamps is displayed in Fig. 1 to show the interaction forces and some essential dimensions for the formulation. Here, the right end of the beam is forced to displace downwards $F_{N\ top}$ and $F_{N\ bottom}$ are the clamp normal forces, including the tightening forces at the top and bottom clamps, respectively and $F_{F\ top}$ and $F_{F\ bottom}$ are the frictional forces at the contact interface between the clamps and the beam, h is the beam thickness, and e is the eccentricity between the resultant normal forces which roots from the non-uniform and different contact pressure distribution at the contact interfaces of the beam, upper and lower clamps. This model consists of a clamped beam system, including friction at the interfaces between the beam and the clamps.

The frictional forces can be defined as functions of the friction coefficient μ and the normal forces $F_{N\ top}$, $F_{N\ bottom}$.

Considering these clamps make an imperfect encastre support, it is predicted that the reactions consist of a moment, horizontal and vertical forces once the actual reactions shown in the free body diagram are simplified to point loads.

The boundary conditions, where the clamps are, completely restrict only the translational degrees of freedom, namely longitudinal and transverse displacements. However, due to the imperfections caused by friction, the rotation is not entirely restricted; instead, a solution-dependent reaction moment is imposed, and the beam cross-section has a partially constrained rotational degree of freedom. The frictional interactions between the beam and the clamps are represented with concentrated reaction loads. These boundary conditions can be expressed:

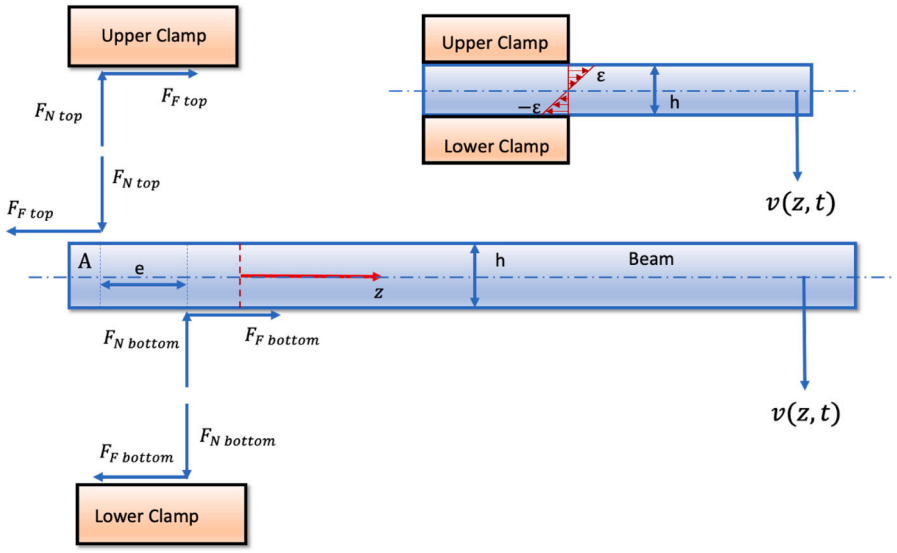

Fig. 1. Free body diagram of a beam with frictional clamps. (The right-hand side of the beam is assumed to be bent downwards.) accompanied by the axial strain distribution along the cross-section at the clamps.

$$v_A = 0, \tag{2a}$$

$$M_A = -EI \left.\frac{\partial^2 v}{\partial z^2}\right|_{z=0}, \tag{2b}$$

Here, a denotes the imposed displacement amplitude, v_A stands for the deflection of the beam at point A, and M_A denotes the resultant at the same location.

The reaction moment is the sum of two parts, as there are two different force couples in the axial and transverse directions. Let these parts of the reaction moment be referred to as M_N and M_F as follows:

$$M_A = M_F + M_N \tag{3}$$

where the subscripts N and F denote the directions of normal and friction forces, respectively by which these moments are brought into existence.

The first part of the reaction moment M_N is caused by the eccentric normal contact forces. The eccentricity e is to be found between the top and bottom resultant normal contact forces due to different contact pressure distributions, which is a consequence of the bending deformation of the beam, as mentioned earlier. While the second part of the component of the reaction moment M_F roots from the existence of friction, which depends on the relative motion between the beam and the clamps. Therefore M_N is conservative, and M_F is dissipative.

Taking a closer look at the normal contact forces $F_{N\ top}$ and $F_{N\ bottom}$ and the mechanism that creates the moment M_N, one can notice that during the vibration of the beam, the normal forces at the top and the bottom beam-clamp interfaces are time-dependent and are not always equal to each other. The difference between these two normal contact forces balances the shear reaction force of the clamp that acts on the beam. Assuming the system is stable, summing the tightening forces with the shear force for each clamp, it becomes clear that, whilst the normal load increases on one clamp, the load on the other clamp relaxes. As a result of changing normal contact forces, $F_{N\ top}$ and $F_{N\ bottom}$, the frictional forces $F_{F\ top}$ and $F_{F\ bottom}$ are affected as well. The maximum frictional forces $\mu F_{N\ top}$ and $\mu F_{N\ bottom}$ have a similar trend as the normal forces. Note that μ represents the coefficient of friction for the contact and is assumed to be constant throughout the whole process. Thus, the change of the normal forces directly affects the maximum frictional forces. Increasing the maximum frictional forces at one contact interface reduces the maximum frictional forces on the other interface for the same support depending on their respective normal forces. However, an average normal force, which can be approximated as the initial tightening force, is seen as representative and denoted with F_N. With a similar approach, the maximum frictional forces can be calculated using the averaged coefficient of friction μ and the averaged normal forces F_N. The averaged frictional forces are indicated as F_F.

Moving forward, the moment M_N can be essentially calculated by multiplying the eccentricity e with the averaged normal force F_N as given in the following expression:

$$M_N = F_N\, e(\phi_A) \tag{4}$$

Here, ϕ_A is the rotation of the cross-section of the beam at the clamp A. Also, the eccentricity e is considered as the variable that controls the change in M_N since F_N is assumed as a constant.

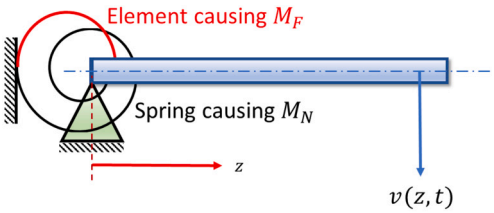

Fig. 2. The representation of the boundary with clamps.

A more useful form to express the conservative first part of the reaction moment M_N would be to formulate a linear, rotational spring, with a stiffness k_N, to calculate the moment. There, the eccentricity e is assumed to be proportional to the rotation of the cross-section ϕ_A and the rest of the parameters are included in the support stiffness. The spring formulation reads:

$$M_N = k_N\ \phi_A \tag{5}$$

Using these assumptions, the second and the last part of the support reaction moment, which roots in the frictional forces, can be formulated. This moment is simply calculated by multiplying the frictional force with the beam thickness as given below (see Fig. 1):

$$M_F = F_F\ h \tag{6}$$

Since the friction forces can remove energy from the system, this part of the reaction moment is evaluated as dissipative.

To clarify the definition of the frictional forces, the relative motion between the beam and the clamps in the system should be defined more precisely. As Euler-Bernoulli beam theory suggests, the cross-section of the beam is rigid, and it is initially perpendicular to the axis and stays so after the deformation. Therefore the motion of the cross-section can be decomposed into translational and rotational motions. The translation of the cross-section is called the deflection, and the rotation of the cross-section is approximated with the first derivative of deflection with respect to the axial coordinate z. The shear deformation of the beam is assumed to be small and neglected during the calculations. As a result, normal strain distribution due to bending deformation along the cross-section is linear. The absolute value of the normal strain reaches its minimum at the neutral axis and its maxima at the boundaries, as displayed in Fig. 1. Thus, the relative motion at the contact interfaces can be defined with the dependence on the normal strain at the boundaries of the beam and the support ε_A. Since the clamps are considered to be stationary, no complicated relative motion calculation is needed to express the relative motion between the clamps and the beam.

After all these steps, the boundary with clamps is visualised in Fig. 2. To restrict the translation of the boundary, simple support is placed. To impose the solution-dependent moments, a rotational spring and a friction element are used.

To sum up, the basic assumptions of the model are listed below:

- **In-Plane Bending Motion:** Considers only the in-plane bending motion of a beam with a uniform rectangular cross-section.
- **Simple Bending Motion:** Focuses on simple bending motion, excluding complex patterns like torsional or coupled bending-torsional vibrations.
- **Small Displacement Assumption:** Assumes small displacements, aligning with linear beam theory and simplifying the mathematical formulation.
- **Use of Euler-Bernoulli Beam Theory:** Employs Euler-Bernoulli beam theory, assuming plane sections remain plane and normal after deformation.
- **Neglect of Shear Deformation:** Assumes shear deformation of the beam is small and is thus neglected, in line with Euler-Bernoulli beam theory assumptions.
- **Symmetric Cross-Section:** Considers that the cross-section of the beam to be symmetric about the plane that the beam axis lies.
- **Uniform Properties of the Beam:** Assumes to have uniform properties, including cross-sectional area, density, elasticity modulus, and area moment of inertia.
- **Linear Elastic Material:** Assumes to be made of a linear elastic material that obeys Hooke's law.
- **No External Load in the Equation of Motion:** Excludes the external load terms from the equation of motion, as excitation and friction are handled in the boundary conditions.
- **Stationary Clamps and Relative Motion Considerations:** Considers clamps as stationary, with relative motion between the beam and clamps defined based on the normal strain at the boundaries.
- **Simplified Frictional Interaction:** Represents frictional forces at the clamps as functions of the friction coefficient and normal forces, assuming a constant coefficient of friction.
- **Imperfect Encastre Support Due to Clamps:** Assumes clamps provide imperfect encastre support, leading to partially constrained rotational freedom and solution-dependent reaction moments.
- **Rotational Spring Representation:** Uses a linear rotational spring to model the conservative part of the reaction moment, with stiffness proportional to the beam's cross-section rotation.

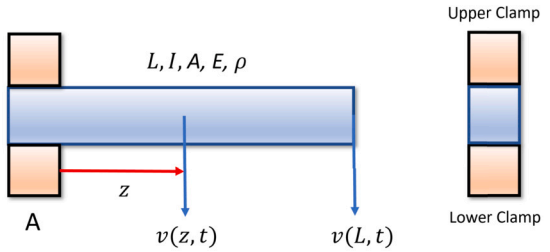

Fig. 3. Schematic visualisation of a cantilever beam.

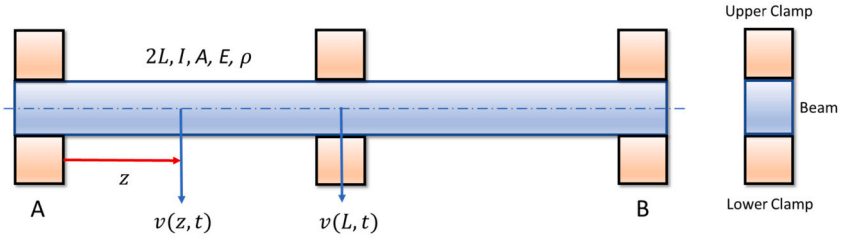

Fig. 4. Schematic visualisation of DMA dual cantilever fixture configuration.

2.1. Cantilever beam

As the first special case, a beam clamped at one end and free at the other is considered. This is one of the models that can represent some of the most common engineering systems, such as turbine blades. Here, a cantilever beam of length L is modelled using the same approach. The cantilever beam system is shown in Fig. 3.

The boundary conditions for a cantilever beam are presented as follows:

$$v(0,t) = 0, \tag{7a}$$

$$\left.\frac{\partial^2 v}{\partial z^2}\right|_{z=0} = -\frac{F_F\, h + k_N \left.\frac{\partial v}{\partial z}\right|_{z=0}}{EI}, \tag{7b}$$

$$v(L,t) = a\cos(\omega t), \tag{7c}$$

$$\left.\frac{\partial^2 v}{\partial z^2}\right|_{z=L} = 0 \tag{7d}$$

Here, $a\cos(\omega t)$ is the imposed displacement in the transverse direction as the external excitation, where a is the displacement amplitude, and ω is the frequency of the imposed motion.

2.2. Dual cantilever beam

The second case is inspired by a very common vibration testing setup that measures the material properties of the sample beam, the dual cantilever fixture configuration of a Dynamic Mechanical Analysis (DMA) experimental setup.

For simplicity, only half of the system is modelled. This means there is only one support at point A at $z = 0$ with two clamps, and the free end does not rotate but is subjected to a displacement. This can be done by taking advantage of the fact that the beam shows exact symmetry about an axis perpendicular to its tangent of the neutral axis at the mid-point located at $z = L$. So, modelling only half of the beam is sufficient to represent its behaviour. A sketch for this beam-fixture assembly can be found in Fig. 4.

Finally, the boundary conditions are expressed as:

$$v(0,t) = 0, \tag{8a}$$

$$\left.\frac{\partial^2 v}{\partial z^2}\right|_{z=0} = -\frac{F_F h + k_N \left.\frac{\partial v}{\partial z}\right|_{z=0}}{EI}, \tag{8b}$$

$$v(L,t) = a\cos(\omega t), \tag{8c}$$

$$\left.\frac{\partial v}{\partial z}\right|_{z=L} = 0 \tag{8d}$$

3. Solution of the formulation with the Jenkins element

3.1. Nondimensionalisation

A beam excited with an imposed harmonic transverse displacement $a\cos(\omega t)$ at $z = L$ is taken into consideration, where a denotes the amplitude. As mentioned earlier, the system obeys the equation of motion given in Equation (1).

Normalisation is performed by defining the system parameters, m, the mass, ω_0, the eigenvalue of the first bending mode, $1/\kappa$, the wavelength of the excitation frequency, $1/\kappa_0$, the wavelength of the corresponding eigenfunction, F_0, the characteristic force, M_0, the characteristic moment, k_F, the stiffness coefficient of the dissipative part of the support reaction based on the Jenkins approach and k_0, the characteristic stiffness of the support reaction at the clamp as presented:

$$\begin{aligned} m = \rho A L;\ \kappa^2 = \omega\sqrt{\rho A/EI};\ \kappa_0^2 = \omega_0\sqrt{\rho A/EI};\\ F_0 = m\,\omega_0^2 L;\ M_0 = F_0\ L;\ k_0 = m\,\omega_0^2 L^2; \end{aligned} \tag{9}$$

Similarly, the nondimensional parameters $\tilde{a}$, $\tilde{h}$, $\tilde{z}$, $\tilde{v}$, $\tilde{t}$, $\tilde{\omega}$, $\tilde{F}_F$, $\tilde{F}_N$, $\tilde{M}_F$, $\tilde{M}_N$, $\tilde{\kappa}$, $\tilde{\kappa}_0$, $\tilde{k}_N$, and $\tilde{k}_F$ are defined taking advantage of the existing system parameters and their characteristic references as shown:

$$\begin{aligned} \tilde{a} = a/L;\ \tilde{h} = h/L;\ \tilde{z} = z/L;\ \tilde{v} = v/L;\ \tilde{t} = t\,\omega_0;\ \tilde{\omega} = \omega/\omega_0;\\ \tilde{F}_F = F_F/F_0;\ \tilde{F}_N = F_N/F_0;\ \tilde{M}_F = M_F/M_0;\ \tilde{M}_N = M_N/M_0;\\ \tilde{\kappa} = \kappa L;\ \tilde{\kappa}_0 = \kappa_0 L;\ \tilde{k}_N = k_N/k_0;\ \tilde{k}_F = k_F/k_0; \end{aligned} \tag{10}$$

Then, the nondimensional form of the equation of motion is obtained as:

$$\ddot{\tilde{v}} - \frac{1}{\tilde{\kappa}_0^4}\tilde{v}^{IV} = 0 \tag{11}$$

The Galerkin method is chosen to solve this problem, and the assumed solution (also referred to as the ansatz) is taken as the usual analytical solution for beams which can be found as follows:

$$\tilde{v}\left(\tilde{z},\tilde{t}\right) = \left(C_1\cos(\tilde{\kappa}\tilde{z}) + C_2\sin(\tilde{\kappa}\tilde{z}) + C_3\cosh(\tilde{\kappa}\tilde{z}) + C_4\sinh(\tilde{\kappa}\tilde{z})\right)\cos(\tilde{\omega}\tilde{t} + \psi) \tag{12}$$

It is also assumed that the frequency range of the imposed harmonic displacement includes the first natural frequency of the beam. Here in the ansatz function, $\tilde{v}$ is the nondimensional displacement of the beam, and ψ denotes the phase.

The application of the Galerkin method requires plugging the assumed solution function into Equation (11), which yields:

$$\left(\frac{\tilde{\kappa}^4}{\tilde{\kappa}_0^4} - \tilde{\omega}^2\right)\tilde{v}\left(\tilde{z},\tilde{t}\right) = 0 \tag{13}$$

The Galerkin method, employed in this study, is applied in the spatial domain. It involves multiplying the residual of the differential equation given in Equation (11) by a set of trial (or weight) functions and integrating over the domain. This process ensures that the residual of the equation, when averaged over the domain with respect to the chosen trial functions, vanishes. In our application, the trial functions are chosen to be the same as the assumed solution functions in Equation (12), satisfying the boundary conditions of the problem. This choice simplifies the process of ensuring that the integrated residual is zero, a fundamental requirement of the Galerkin method. The resulting expressions, as derived from this procedure, lead to Equation (13), where the form of the solution function inherently satisfies the boundary conditions and the differential equation, thus ensuring the validity of the Galerkin approach in this context.

3.2. Solution of the frictional clamp-beam system

The friction depends on the slip itself for the Jenkins approach. Therefore, it is necessary to use the relation between the slip and the maximum normal strain which correlates to the rotation of the cross-section, as described earlier.

The primary difference between the full-stick and full-slip regimes is the external/friction load definition. The frictional load for the stick regime can be obtained by substituting the solution into the moment equation:

$$\tilde{M}_F(\tilde{t}) = \tilde{k}_F\phi_A \tag{14}$$

Similarly, in the slip regime, the frictional load is constant and equals to the maximum frictional moment, which is given by:

$$\tilde{M}_F(\tilde{t}) = \mu\tilde{F}_N\tilde{h} \tag{15}$$

To determine the limits of the full-stick and full-slip regimes, their moment equations can be used considering, at their limits, the frictional moment for the full-stick has to be equal to the moment for the full-slip regimes. This expression reads:

$$\tilde{k}_F\phi_A = \mu\tilde{F}_N\tilde{h} \tag{16}$$

To perform the full solution for both regimes, boundary conditions are required. Therefore, the two cases are solved separately. However, the approach remains the same.

3.2.1. Cantilever beam

In this case, the free end of the beam is excited harmonically displacement function $a\cos(\omega t)$, whilst the frictional clamps on one end completely restrain the transverse motion. However, as explained earlier, the rotation is not entirely restricted because of the contact at the beam-clamp interfaces. Thus, the nondimensional boundary conditions are obtained as:

$$\tilde{v}\left(0,\tilde{t}\right)=0, \tag{17a}$$

$$\left.\frac{\partial^2\tilde{v}}{\partial\tilde{z}^2}\right|_{z=0}=-\tilde{\kappa}_0^4\left(\tilde{F}_F\tilde{h}+\tilde{k}_N\phi_A\right), \tag{17b}$$

$$\tilde{v}\left(1,\tilde{t}\right)=\tilde{a}\cos(\tilde{\omega}\tilde{t}), \tag{17c}$$

$$\left.\frac{\partial^2\tilde{v}}{\partial\tilde{z}^2}\right|_{\tilde{z}=1}=0 \tag{17d}$$

Plugging the assumed solution function in Equation (12) into the boundary conditions presented in Equation (17), the coefficients C_1, C_2, C_3 and C_4 are solved for each regime. Then, the rotation at the clamp ϕ_A in full-stick and full-slip regimes are determined as:

$$\phi_{A\ stick}=\frac{\tilde{a}\tilde{\kappa}^2\left(\sin\left(\tilde{\kappa}\right)+\sinh\left(\tilde{\kappa}\right)\right)}{\tilde{\kappa}_0^4\left(\tilde{k}_N+\tilde{k}_F\right)\left(\cos\left(\tilde{\kappa}\right)\sinh\left(\tilde{\kappa}\right)-\sin\left(\tilde{\kappa}\right)\cosh\left(\tilde{\kappa}\right)\right)+2\tilde{\kappa}\sin\left(\tilde{\kappa}\right)\sinh\left(\tilde{\kappa}\right)}\cos\left(\tilde{\omega}\tilde{t}\right) \tag{18a}$$

$$\phi_{A\ slip}=\frac{\tilde{a}\tilde{\kappa}^2\left(\sin\left(\tilde{\kappa}\right)+\sinh\left(\tilde{\kappa}\right)\right)+\mu\tilde{F}_N\tilde{h}\tilde{\kappa}_0^4\left(\sin\left(\tilde{\kappa}\right)\cosh\left(\tilde{\kappa}\right)-\cos\left(\tilde{\kappa}\right)\sinh\left(\tilde{\kappa}\right)\right)}{\tilde{\kappa}_0^4\tilde{k}_N\left(\cos\left(\tilde{\kappa}\right)\sinh\left(\tilde{\kappa}\right)-\sin\left(\tilde{\kappa}\right)\cosh\left(\tilde{\kappa}\right)\right)+2\tilde{\kappa}\sin\left(\tilde{\kappa}\right)\sinh\left(\tilde{\kappa}\right)}\cos\left(\tilde{\omega}\tilde{t}\right) \tag{18b}$$

Here, it is important to note that the phase lag is found as zero due to the nature of the Jenkins approach as presented:

$$\psi=0 \tag{19}$$

As explained in the previous section, to spot the limits of these two distinct regimes, one can insert the first spatial derivative of Equation (12) into Equation (16). Using these relations, the imposed displacement amplitude at the full-stick and full-slip regime limits $\tilde{a}^*$ is determined as follows:

$$\tilde{a}^*=\mu\tilde{F}_N\tilde{h}\,\frac{\tilde{\kappa}_0^4(\tilde{k}_N+\tilde{k}_F)\left(\cos\left(\tilde{\kappa}\right)\sinh\left(\tilde{\kappa}\right)-\sin\left(\tilde{\kappa}\right)\cosh\left(\tilde{\kappa}\right)\right)+2\tilde{\kappa}\sin\left(\tilde{\kappa}\right)\sinh\left(\tilde{\kappa}\right)}{\tilde{\kappa}^2\tilde{k}_F\left(\sin\left(\tilde{\kappa}\right)+\sinh\left(\tilde{\kappa}\right)\right)} \tag{20}$$

3.2.2. Dual cantilever beam

Here, the mid-point of the beam is forced to move with a harmonic displacement function $a\cos(\omega t)$. The clamps behave exactly the same as in the cantilever case in terms of restricting the transverse deflection and rotation since the friction forces are defined the same way as in the previous section.

The dual cantilever beam can be solved using the same approach with only a quite minor difference in the boundary conditions. Similar to the cantilever case, using these assumptions/conditions, the nondimensional boundary conditions can be written as:

$$\tilde{v}\left(0,\tilde{t}\right)=0, \tag{21a}$$

$$\left.\frac{\partial^2\tilde{v}}{\partial\tilde{z}^2}\right|_{z=0}=-\tilde{\kappa}_0^4\left(\tilde{F}_F\tilde{h}+\tilde{k}_N\phi_A\right), \tag{21b}$$

$$\tilde{v}\left(1,\tilde{t}\right)=\tilde{a}\cos(\tilde{\omega}\tilde{t}), \tag{21c}$$

$$\left.\frac{\partial\tilde{v}}{\partial\tilde{z}}\right|_{\tilde{z}=1}=0 \tag{21d}$$

Substituting the ansatz in Equation (12) into the expressions of the boundary conditions in Equation (21), the unknowns C_1, C_2, C_3 and C_4 are determined for full-stick and full-slip regimes.

$$\phi_{A\ stick}=\frac{\tilde{a}\tilde{\kappa}^2\left(\cos\left(\tilde{\kappa}\right)-\cosh\left(\tilde{\kappa}\right)\right)}{\tilde{\kappa}_0^4\left(\tilde{k}_N+\tilde{k}_F\right)\left(1-\cos\left(\tilde{\kappa}\right)\cosh\left(\tilde{\kappa}\right)\right)+\tilde{\kappa}\left(\cos\left(\tilde{\kappa}\right)\sinh\left(\tilde{\kappa}\right)-\sin\left(\tilde{\kappa}\right)\cosh\left(\tilde{\kappa}\right)\right)} \tag{22a}$$

$$\phi_{A\ slip}=\frac{\mu\tilde{F}_N\tilde{h}\tilde{\kappa}_0^4\left(1-\cos\left(\tilde{\kappa}\right)\cosh\left(\tilde{\kappa}\right)\right)+\tilde{a}\tilde{\kappa}^2\left(\cosh\left(\tilde{\kappa}\right)-\cos\left(\tilde{\kappa}\right)\right)}{-\tilde{\kappa}_0^4\tilde{k}_N\left(1-\cos\left(\tilde{\kappa}\right)\cosh\left(\tilde{\kappa}\right)\right)+\tilde{\kappa}\left(\sin\left(\tilde{\kappa}\right)\cosh\left(\tilde{\kappa}\right)-\cos\left(\tilde{\kappa}\right)\sinh\left(\tilde{\kappa}\right)\right)} \tag{22b}$$

Similar to the cantilever case, there is no phase lag due to frictional damping and the nature of the Jenkins approach.

Following the same steps as in the cantilever case, the imposed displacement amplitude that brings the system to the full-stick and full-slip regime limits $\tilde{a}^*$ reads:

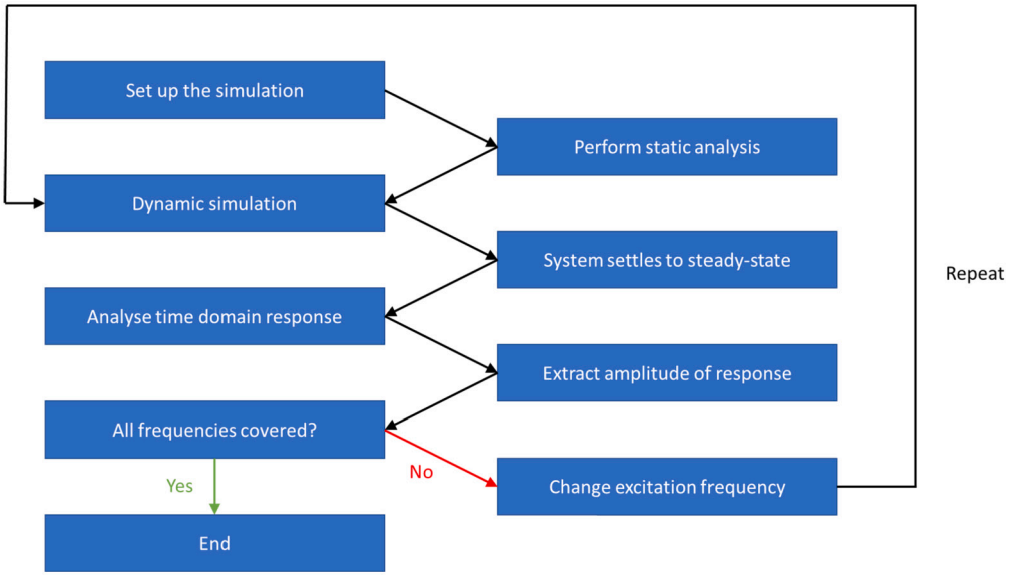

Fig. 5. Schematical visualisation of the algorithm used in the numerical approach.

$$\tilde{a}^* = \mu \tilde{F}_N \tilde{h} \, \frac{\tilde{\kappa}_0^4 \left(\tilde{k}_N + \tilde{k}_F\right)\left(1 - \cos\left(\tilde{\kappa}\right)\cosh\left(\tilde{\kappa}\right)\right) + \tilde{\kappa}\left(\cos\left(\tilde{\kappa}\right)\sinh\left(\tilde{\kappa}\right) - \sin\left(\tilde{\kappa}\right)\cosh\left(\tilde{\kappa}\right)\right)}{\tilde{\kappa}^2 \tilde{k}_F \left(\cos\left(\tilde{\kappa}\right) - \cosh\left(\tilde{\kappa}\right)\right)} \tag{23}$$

4. Numerical modelling

4.1. Description of the numerical modelling approach

Unlike the analytical model, the numerical model follows a completely different workflow and has different assumptions. The numerical workflow involves performing a frequency sweep using the time marching approach, which is a very basic method to analyse the vibrations of such nonlinear systems. First, a static analysis of the tightening of the clamps is performed. This process is followed by a time domain dynamic simulation with an implicit solver exciting the system using the middle/moving clamps monoharmonically by a predefined displacement amplitude. After the system settles to a steady state, the time domain response of a node from the beam in contact with the clamp is analysed. The amplitude of the time domain response is extracted for that frequency, and then the frequency of excitation is changed, and the whole process is repeated until the desired data is acquired. This structure of the numerical modelling is executed by employing Python scripting in a commercial finite element software package, Abaqus. A visualisation of the algorithm of the numerical method is presented in Fig. 5.

The Jenkins contact elements are inserted between the matching contact nodes on both ends of the beam in the finite element model. The contact between the beam and the middle clamp is defined as frictionless hard contact to achieve consistency with the analytical formulation considering this moving clamp is not taken into account in the analytical model. The numerical section of this study involves a three-dimensional finite element model, whilst the analytical model consists of a one-dimensional beam equation. Thus, the complicated assumptions on the contact elements of the analytical model are replaced by the conventional Jenkins element in three dimensions. A more detailed description of the Jenkins contact elements is to be found in the next section.

For consistency with the analytical model, the material damping is disregarded in the numerical model. However, it is known that Abaqus has a default numerical/artificial damping defined in its built-in structure to achieve numerical stability. Besides, the implicit solver scheme, by nature, may introduce a kind of artificial damping to the system. Therefore, whilst the only source of damping in the analytical model is friction, this is not the case for the numerical model. Even though a minor contribution to the damping by this artificial damping is expected, this still has to be noted.

4.2. Modelling of nonlinear frictional force with the Jenkins model

Friction is modelled using the Jenkins model, which represents the behaviour through relative displacement between two points of contact. In this case, the nonlinear force reaches the tangential friction force μF_N for large relative motion. For minimal relative motion, the contact is modelled as a force linearly associated with the chosen parameter.

Hence, the frictional contact force $F_R(w_{rel})$ is represented as:

$$F_{NL}(w_{rel}) = \begin{cases} -\mu F_N & \text{for } F_R(w_{rel}) < -\mu F_N \\ +\mu F_N & \text{for } F_R(w_{rel}) > +\mu F_N \\ F_R(w_{rel}) & \text{otherwise} \end{cases} \tag{24}$$

Table 1
Material properties used for the numerical example.

Material Properties	Steel	Epoxy
Density $[kg/m^3]$	7800	1400
Young's Modulus $[GPa]$	210	3.5
Poisson's Ratio	0.28	0.38

Here, F_{NL} denotes the nonlinear force, F_N indicates the normal force in the contact, and w_{rel} is the relative displacement, slip.

In the Jenkins model, the frictional contact force F_R follows an elastic behaviour similar to the spring formulation. Therefore, F_R is given by:

$$F_R = k_T(w_{rel} - \Delta w_{slip}) \tag{25}$$

Here, k_T denotes the tangential contact stiffness, and Δw_{slip} is the cumulative relative displacement during slip. The value of Δw_{slip} is obtained via time discretisation, updating its value at each time step of the slip phase.

Assuming the relative displacement is purely harmonic:

$$w_{rel}(t) = a\cos(\omega t). \tag{26}$$

Stick-slip cycle is observed when $k_T\, a$ surpasses the friction limit μF_N, else Δw_{slip} is given by:

$$\Delta w_{slip} = -\text{sign}(\dot{w}_{rel})(a - \frac{\mu F_N}{k_T}) \tag{27}$$

Thus, the frictional contact force is:

$$F_R = \begin{cases} k_T\, a\cos(\omega t) - (k_T\, a - \mu F_N) & \text{for } t \in [0, T/2] \\ k_T\, a\cos(\omega t) + (k_T\, a - \mu F_N) & \text{for } t \in [T/2, T] \end{cases}. \tag{28}$$

If $k_T\, a < \mu F_N$, a full-stick cycle occurs with no dissipation, indicating a purely elastic frictional force. Fig. 6 illustrates a generic stick-slip cycle, highlighting different conditions for the friction force. The enclosed area in the hysteresis loop signifies the dissipated energy, which reduces to zero for a pure stick cycle.

5. Numerical example for the dual cantilever model: dynamic mechanical analysis fixture

In this study, only one numerical example is considered for conciseness which is a dual cantilever beam case. Based on the similarity of the physical and also the derived mathematical expressions of cantilever and dual cantilever beams, it can be easily understood that the results of a potential example to be solved with the cantilever beam case, would also be quite comparable and relatable.

This example represents the DMA test setup with the dual cantilever fixture configuration. The fixtures of the DMA are known to be made of stainless steel, and the beam samples are made of epoxy. The material properties are given in Table 1. The beam is 70 mm long and 14 mm wide with a thickness of 4 mm, whilst the clamps have a rectangular surface with dimensions 14 mm by 8 mm in contact with the beam. Fig. 7 displays the finite element model that is used as the input for the numerical method.

This test case is set up with the parameters of the actual DMA test rig at Imperial College London Department of Mechanical Engineering (TA DMA Q800) excited with the maximum displacement possible for the machine. Thus the contact stiffnesses are picked as $k_F = 10^6\ N\ m/rad$ and $k_N = 10^8\ N\ m/rad$. The tightening force is assumed to be $F_N = 20\ N$. Finally, based on the results of Coulomb experiments carried out on the steel-epoxy material pairs, the coefficient of friction is assumed as the coefficient of friction as 0.4.

6. Results and discussion of the numerical example

6.1. Comparison of the analytical formulation against the numerical model

The analytical model calculates the solutions based on two distinct full-stick and full-slip regimes, and this transition between stick and slip regimes is crucial in understanding the vibrational behaviour of the system under different external excitations. The solutions of these regimes are represented with a sketch displayed in Fig. 8. The physically correct solution is the one with the lower amplitude for the selected frequency based on the minimum energy principle. Hence, one could expect to see slip around resonance and stick for the frequencies that are further away from the resonance.

The results of the model built to represent the dual cantilever fixture configuration of the DMA test setup are given in Fig. 9. This figure is prepared with the parameters selected to fit the mentioned DMA rig. Here, the rotational degrees of freedom of the beam at the clamps are of interest. Thus, the y-axis (Amplitude (ϕ)) is plotted. The first point to notice is that the peak is between the nondimensional frequency values of 0.7 and 0.75. This is because the reference natural frequency corresponds to the first bending

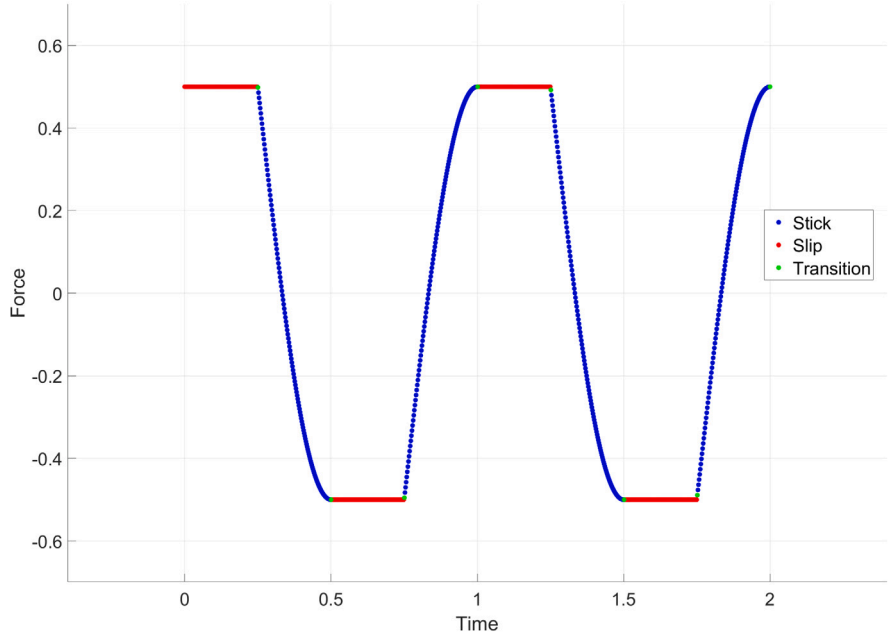

(a) Force against time

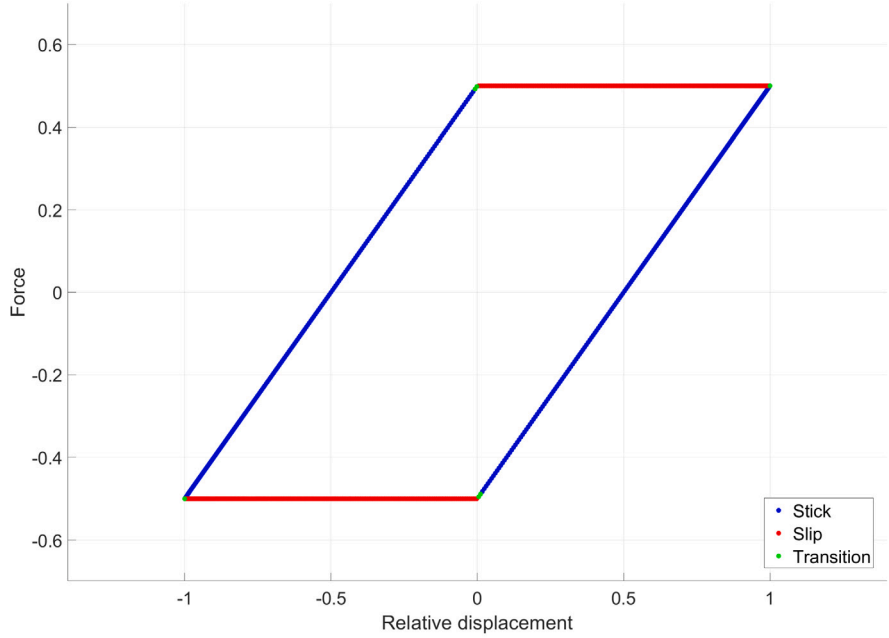

(b) Force against relative displacement

Fig. 6. Behaviour of the Jenkins element under the single harmonic assumption.

mode of the beam when both ends are perfectly fixed. However, the beam-clamp system here cannot completely restrict the rotational degrees of freedom of both ends of the beam. Hence, the system is softer than an ideal dual cantilever beam. Also, the value 0.7 is not any value that the system shows softened behaviour coincidentally. It is important to note that the ratio of the natural frequencies that correspond to the first bending modes for a simply supported beam and a beam fixed at both ends is approximately 0.67. Thus, the value 0.7 suggests that the beam acts more as if it is simply supported instead of an ideally fixed beam at both ends, which leads

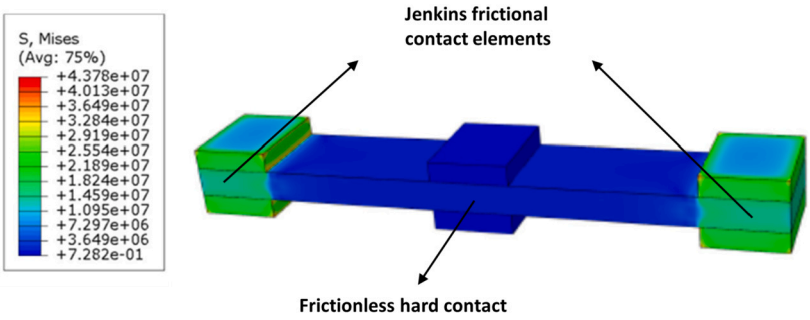

Fig. 7. Finite element model of the dual cantilever fixture.

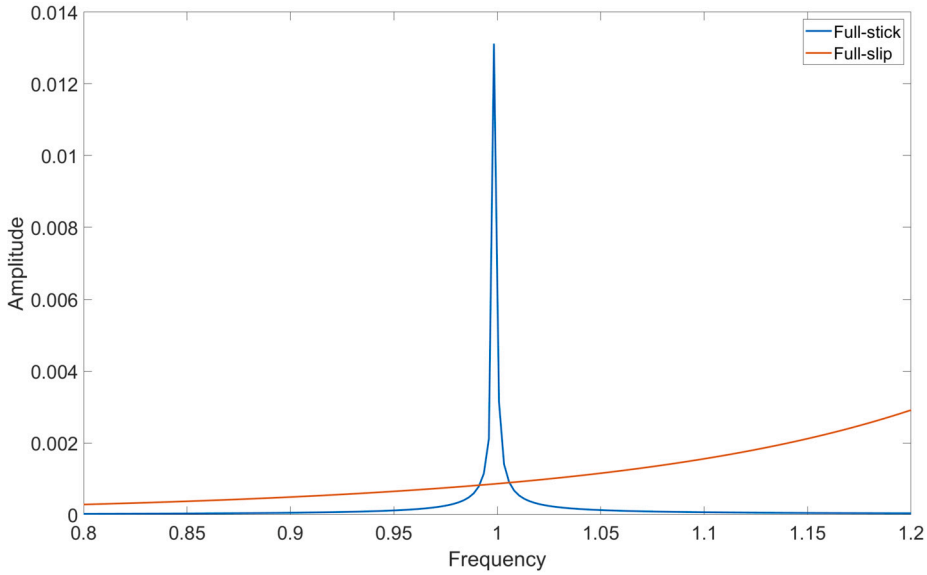

Fig. 8. A sketch of the analytical solutions for the dual cantilever beam in bending motion under the same and constant excitation amplitude.

to this softening. Furthermore, as indicated by Fig. 8, the characteristics of the slip behaviour can be observed around this peak. At lower and higher frequencies, the full-stick regime is dominant. Only around the resonance slip occurs.

In this context, friction emerges as a key factor in restraining the system, especially around the resonance frequency. When excited around the resonance, it is harder to restrict the system due to increased energy inputs leading to greater system responses. Furthermore, the rotation of the beam's cross-section increases as the beam approaches its resonance, which consequently increases the value of the term $\tilde{k}_F\phi$ closer to the limit of the frictional slip. Once the slip takes over, energy dissipation starts, which prevents the amplitude of the rotational degree of freedom of the beam from growing further.

Moreover, it is also observed that with increasing excitation levels, the rotation at the clamps also increases alongside the slope of the full-slip regime curves. This underscores the role of energy input in determining system behaviour.

Comparing the results of the analytical and numerical models, it is found that they are in good agreement, which supports the validity of both approaches. However, the analytical model slightly overshoots what the numerical model predicts with around $3-8\%$ difference overall. The full-stick regime, however, is predicted with more accuracy where the maximum error is found to be slightly more than 3%. Meanwhile, the margins of error are larger for the slip regime, rising up to 8%. These differences are primarily caused by the difference in basic assumptions and significantly different natures of the analytical and numerical models. The analytical model assumes two distinct full-stick and full-slip regimes, whereas the numerical model has a more complex stick-slip approach, as described earlier. In this regard, for this example, the transition regime (stick-slip) appears not to be significant since the results of the numerical model also look quite sharp. If the transition regime had more impact, the numerical model should have captured smoother behaviour around the borders of the full-stick and full-slip regions. Another important difference is the artificial damping that the numerical model has due to the construction of the software Abaqus as explained earlier in Section 4.1. Thus, it is understandable that the results obtained with Abaqus are more damped compared to the analytical model's results considering the analytical model only accounts for friction as the source of damping, whereas Abaqus adds some kind of artificial damping to the system by the definition of the elements as well as the implicit dynamic solver.

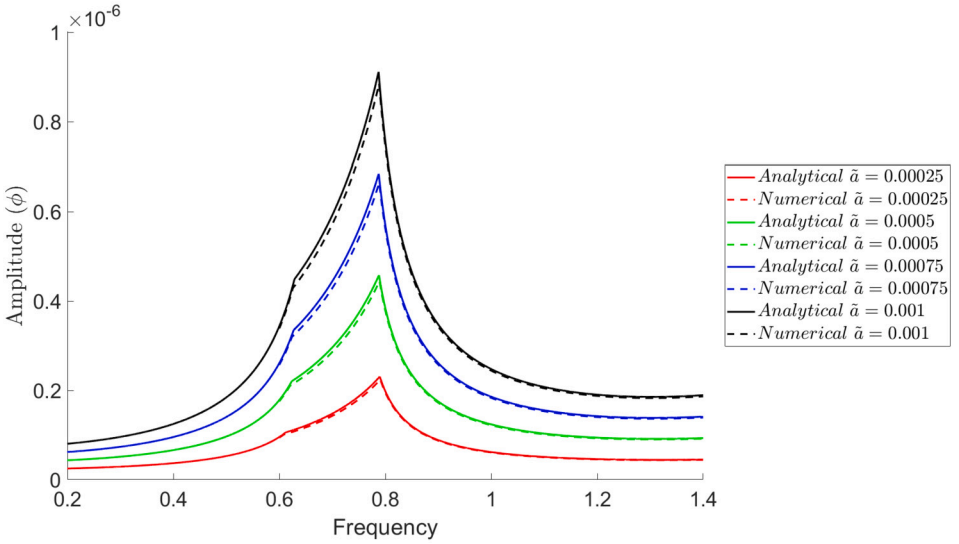

Fig. 9. Comparison of analytical and numerical results for the dual cantilever beam case under the same and constant excitation amplitude.

For this very specific case of dual cantilever fixture configuration of the DMA test setup, it is also important to note that the analytical model does not consider the moving clamps, which are located in the middle of the beam, whilst the numerical model includes these components. However, the contact definition in the numerical analysis is frictionless contact that does not allow penetration. Therefore it is judged that the impact of the inclusion of these moving clamps in the numerical model on the results remains limited. Understanding the system's vibrational behaviour in this manner is crucial in DMA setups as well as in many other engineering applications, allowing for better prediction of the system behaviour, and again, for this particular case, the interpretation of test results and guiding adjustments to test parameters for optimal preparation of the experimentation process.

Furthermore, there are studies in the literature that observed similar physical behaviours with frictional systems. Ciğeroğlu and Özgüven investigate the dynamic behaviour of bladed discs with friction [84]. In that study, they reveal a similar stick and slip phenomenon in Figures 9 and 10. Similarly, Marino and Cicirello, observed the same behaviour for a discrete mass-spring system in Figures 13 and 19 [85].

Despite the slight differences in the results, the analytical model serves as a valuable tool, providing an easier and faster way to understand the basic behaviour of the system. For a more detailed analysis, however, the numerical model is essential as it can account for more complex system interactions.

6.2. Parametric investigation

After the comparison of the analytical model against the numerical model with fewer simplification assumptions, it is understood that the analytical model is accurate. Therefore, the effects of the mechanical system parameters are investigated, taking advantage of the analytical formulation. The DMA test setup is used for the parametric study. The material properties and the contact parameters are kept the same unless stated otherwise.

First, the clamping stiffness parameters, k_N and k_F, are brought to the spotlight. Figs. 10 and 11 display the changes in the forced response of the clamp-beam system against changes in the clamping stiffness parameters. The correlation between the dynamic response and the clamping stiffnesses appears to be quite complicated. For each set of parameters, the frequency response curves look significantly different.

Fig. 10 shows the response of the clamp-beam system for lower values of k_F and k_N. In all three plots, the rotation amplitudes drop as the stiffness values grow. In Figs. 10a and 10b, the most significant thing to note is that the peak frequencies shift towards the nondimensional frequency value of 1 as k_F is increased. Unlike Figs. 10a and 10b, in Figs. 10c, the peaks do not shift and are around the nondimensional frequency value of 0.7. Furthermore, the gradient of the curve in the slip regime turns from positive to negative as the stiffness k_F rises. Another thing to mention is that when $k_N = 10^4\ N\ m/rad$ and $k_F = 10^5 N\ m/rad$, as well as when $k_N = 10^3\ N\ m/rad$ and $k_F = 10^4 N\ m/rad$ transition from slip to stick after the peak is quite smooth and cannot be spotted by the naked eye. This points out that the ratio of clamping stiffness is an important factor for the clamp-beam system.

Similar trends can also be observed in Fig. 11. When $k_F = 10^5\ N\ m/rad$ (Fig. 11a), The smooth transition from initial stick to slip disappears with increasing k_N. This smooth transition characteristics are also spotted in Fig. 11b when $k_F = 10^6\ N\ m/rad$, $k_N = 10^5\ N\ m/rad$ and $k_N = 10^6\ N\ m/rad$. Moreover, Fig. 11c displays a similar tendency to Fig. 10c. The vibration amplitudes decline with rising clamping stiffness.

As one of the most interesting outcomes of this study, the peaks in Figs. 11a and 11b shift towards the nondimensional frequency value of 0.7 from 1, in contrast to Figs. 10a and 10b. This, at first glance, seems unusual since here, k_N and k_F are perceived to collectively contribute to the total clamping stiffness of the beam, potentially leading to the expectation that they should introduce

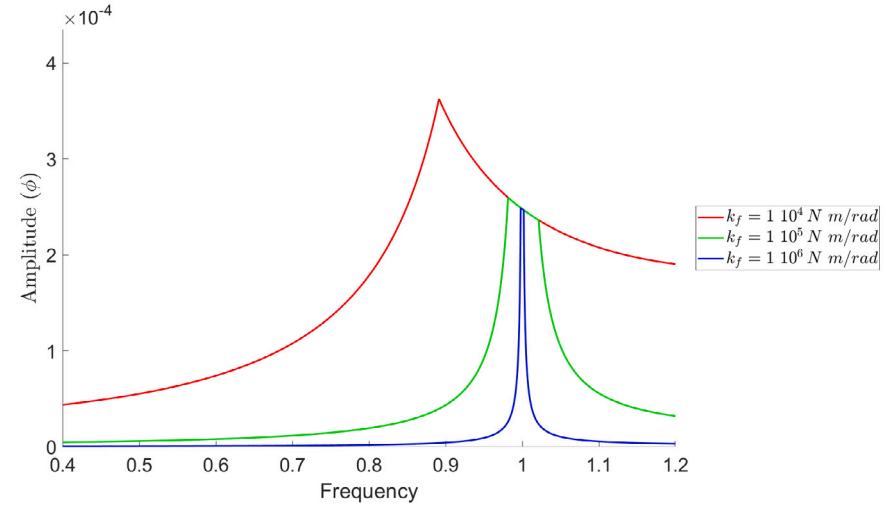

(a) $k_N = 10^3\ N\ m/rad$

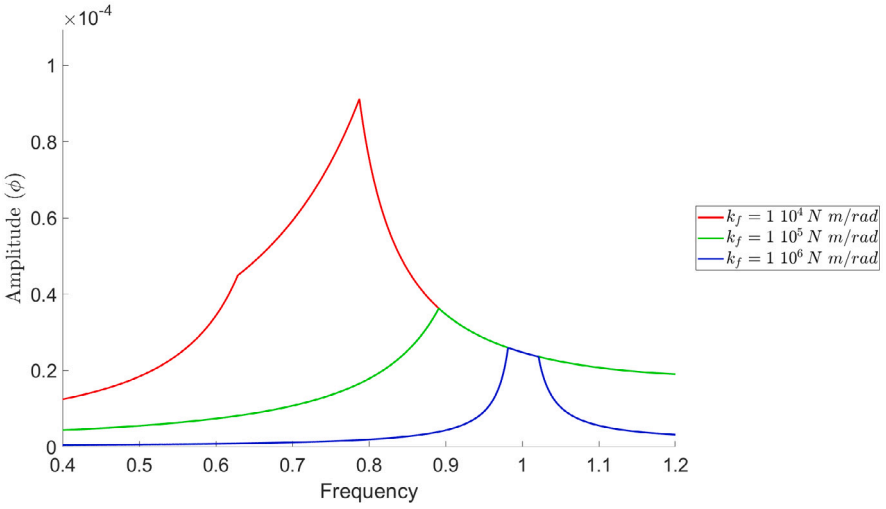

(b) $k_N = 10^4\ N\ m/rad$

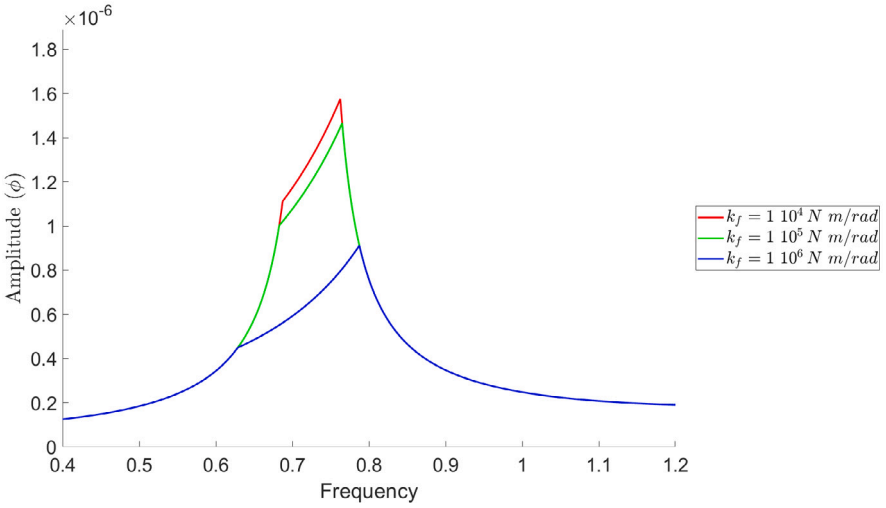

(c) $k_N = 10^6\ N\ m/rad$

Fig. 10. Variation of the dynamics/frequency response of the clamp-beam system based on the contact stiffnesses k_F and k_N under the same and constant excitation amplitude.

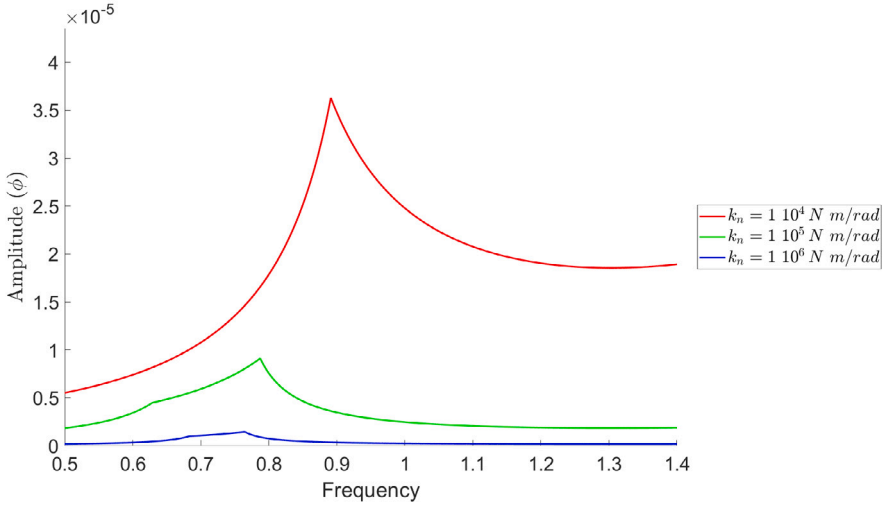

(a) $k_F = 10^5\ N\ m/rad$

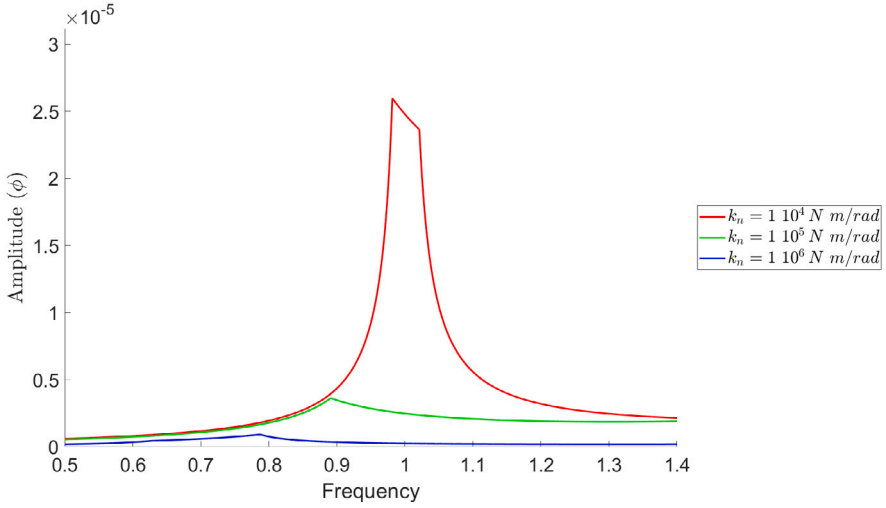

(b) $k_F = 10^6\ N\ m/rad$

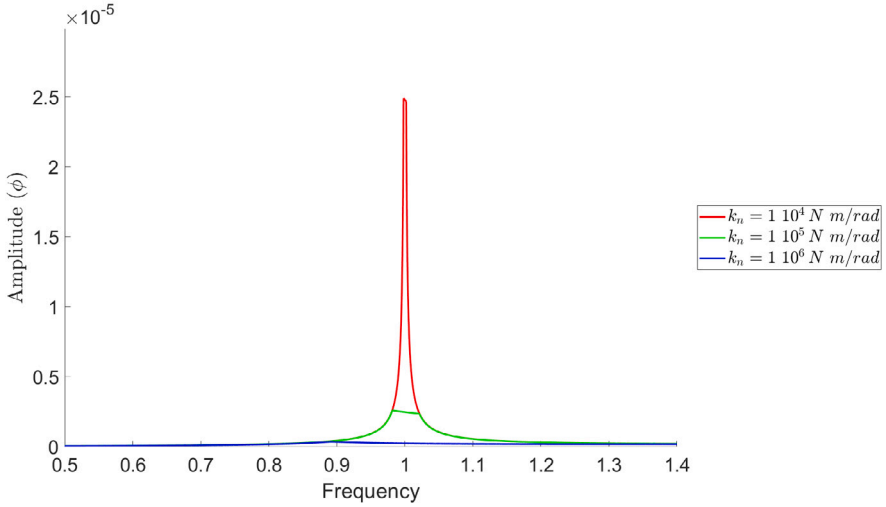

(c) $k_F = 10^7\ N\ m/rad$

Fig. 11. Variation of the dynamics/frequency response of the clamp-beam system based on the contact stiffnesses k_F and k_N under the same and constant excitation amplitude.

similar effects. Nonetheless, a deeper examination of their inherent physical mechanisms and the properties of the mathematical formulation reveals a more complicated relationship. The stiffness parameter k_N is associated with the normal contact stiffness between the beam and the clamp, essentially representing the elastic response of the clamp-beam system to bending. On the other hand, k_F corresponds to the stiffness of the frictional component of the clamp-beam contacts, governing the stick and slip phenomena at the contact, and thereby causing the mechanism for the energy dissipation within the system. Despite contributing to the overall clamping stiffness, k_N and k_F lead to two distinct physical mechanisms within the dynamic system, thus making the ratio of k_F to k_N a significant factor for the determination of the overall system behaviour.

Mathematically, the derived expressions for amplitudes in the full-stick and full-slip phases exhibit the complex relationship between k_N, k_F and the system dynamics. The full-stick regime amplitude is proportional to $\tilde{\kappa}^2/(\tilde{\kappa}_0^4(\tilde{k}_N + \tilde{k}_F))$, indicating that the system's response in the stick regime is dependent on the sum of k_N and k_F. However, in the slip regime, the amplitude is influenced by the term $-\tilde{\kappa}_0^4\tilde{k}_N$, highlighting that the normal contact stiffness directly affects the slip response. The shift in the system dynamics as the ratio k_F/k_N changes is evident in the derived mathematical expressions.

More specifically, the resonance frequency seems to approach a nondimensional frequency value of 1 when $k_F/k_N > 1$, whereas it drops towards a value around 0.7 when $k_F/k_N < 1$.

To understand and explain this behaviour, it is crucial to analyse the underlying physics of the system. With $k_F/k_N > 1$, the frictional effects represented by k_F dominate, pushing the resonance closer to the natural frequency of a beam ideally fixed at both ends, approaching to a nondimensionalised frequency value of 1. On the other hand, when $k_F/k_N < 1$, the influence of the normal stiffness k_N becomes more dominant. Given that k_N is related to the elastic response of the normal component of the contact's behaviour, efficient energy storage and subsequent release due to the springs' elasticity causes the resonance frequency to decrease.

The existence of resonance is predominantly predicated on the equilibrium between energy storage and dissipation mechanisms. The introduction of frictional force and stiffness (k_F) incorporates an energy dissipation mechanism that shifts/modulates this natural frequency. The opposition to the system's motion, due to friction, effectively limits the system's response speed, making the resonance appear at a lower frequency.

Explaining this further from a mathematical perspective, one must consider the analytical solutions of the problem. The amplitude of oscillation, which reaches its peak at resonance, is defined by $\phi_{A\ stick}$ in the stick regime and $\phi_{A\ slip}$ in the slip regime. The formulations for these two regimes are presented in Equation (22). Both $\phi_{A\ stick}$ and $\phi_{A\ slip}$ equations exhibit $\tilde{k}_F$ and $\tilde{k}_N$ in the denominator. Thus, an increase in these parameters leads to a decrease in the amplitude of vibration and vice versa. However, it is imperative to recognise that $\tilde{k}_F$ and $\tilde{k}_N$ do not have equal weight in these expressions. The influences of k_F and k_N are not only different but also interdependent, thereby resulting in a complicated correlation between the k_F/k_N ratio and the resonance frequency.

When $k_F/k_N > 1$, k_F becomes the dominant term, implying that the dissipation ensuing from the frictional forces encapsulated by k_F drives the resonance frequency closer to the reference natural frequency for the system. Whereas, when $k_F/k_N < 1$, the 'elastic' forces indicated by k_N gain dominance. This leads to a more efficient reversible energy storage, which decreases the resonance frequency. Hence, it can be concluded that the ratio k_F/k_N plays a critical role in determining the resonance frequency of the system.

Finally, to reveal the effects of the maximum friction force, Fig. 12 is presented. Expanding and shrinking the slip phase can briefly summarise the impact of the maximum friction force on the dynamics of the clamp-beam system. However, the maximum friction force also affects the system in different ways depending on the stiffness values/ratios. In the scenario where the stiffness values are defined as $k_F = 10^6\ N\ m/rad$ and $k_N = 10^4\ N\ m/rad$ (Fig. 12a), the maximum friction force primarily influences the slope of the full-slip regime curve around the resonance. It is seen that the increased maximum friction force values lead to steeper curves for the full-slip phase of the motion. As one would expect, the maximum friction force has no significant impact on the full-stick regime other than slightly changing the full-stick and full-slip regime boundaries due to the changed gradient of the full-slip part of the frequency response curve. In Fig. 12b, where the stiffness values are assigned as $k_F = 10^6\ N\ m/rad$, and $k_N = 10^5\ N\ m/rad$, the first thing to notice is that the transition from initial full-stick to full-slip is smooth and not really noticeable in the forced response curves. However, the transition from full-slip to full-stick after the resonance is sharp and more obvious. There is also an increase in the peak vibration amplitudes with greater maximum friction force values, which leads to the expansion of the full slip regime. Furthermore, it is found that the vibration amplitudes decrease more and settle to a lower value in curves with higher maximum friction forces as the excitation frequency moves to higher frequencies further away from the resonance. Fig. 12c shows the evolution/shift of the initial full-stick to full-slip transition from being nonsmooth to smooth with increasing maximum friction force. Similar to the previous plot, Fig. 12b, the full-slip regime expands with increasing maximum friction forces as well as the vibration amplitudes drop more in curves corresponding to higher maximum friction force values in higher frequencies.

In examining the model's sensitivity to the clamping stiffnesses, k_N and k_F, alongside the maximum friction force, μF_N, it becomes apparent that these parameters considerably influence the system's dynamics. The interaction of k_N and k_F establishes a dynamic balance between energy storage and dissipation, which is crucial in determining the resonance frequency. A higher k_F/k_N ratio tends to shift the resonance towards the natural frequency of an ideally fixed beam, whereas a lower ratio results in a decrease in resonance frequency, indicative of the dominant influence of elastic forces. Furthermore, the maximum friction force, μF_N, adds a layer of complexity by influencing the transitions between full-stick and full-slip regimes and affecting vibration amplitudes. This response of the system to variations in k_N, k_F, and μF_N highlights the intricate relationship between mechanical properties and dynamic behaviour, underscoring the need for a circumspect approach in interpreting these results. The interdependencies and the model's sensitivity to these critical parameters highlight the importance of further detailed analysis to fully comprehend the implications of parameter variations on the system's behaviour.

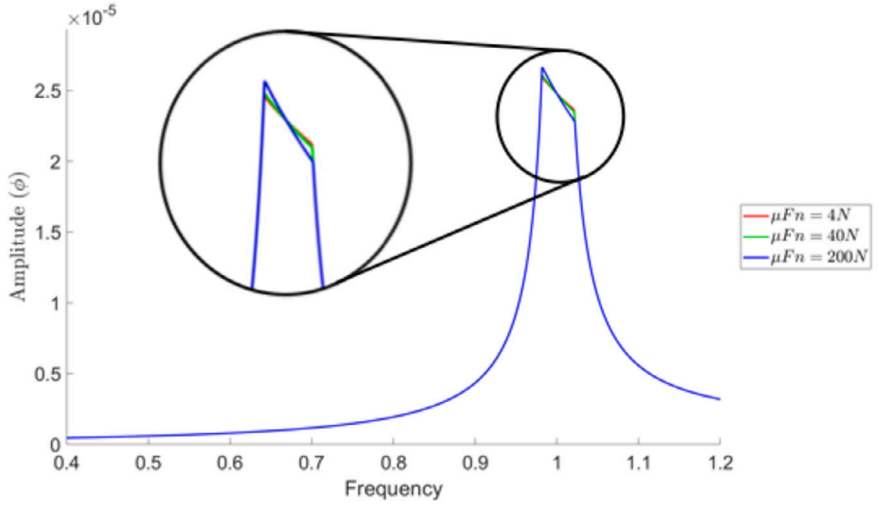

(a) $k_F = 10^6\ N\ m/rad\ ,\ k_N = 10^4\ N\ m/rad$

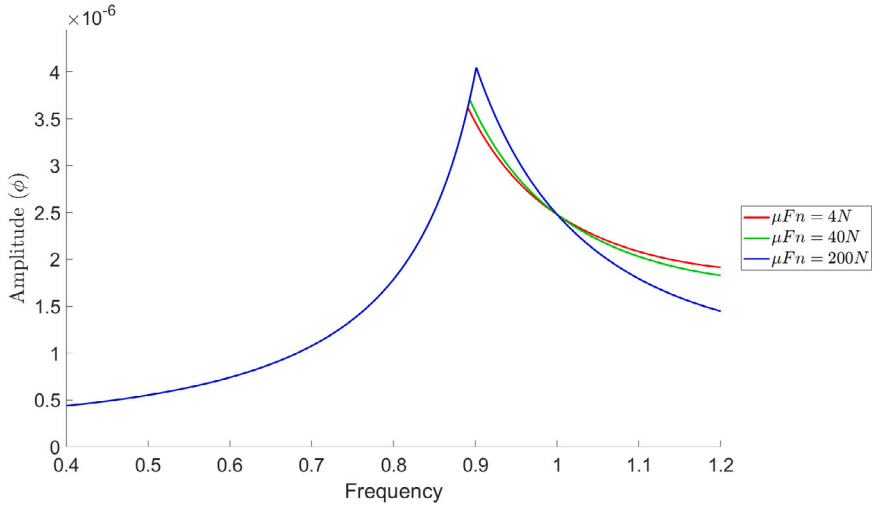

(b) $k_F = 10^6\ N\ m/rad,\ k_N = 10^5\ N\ m/rad$

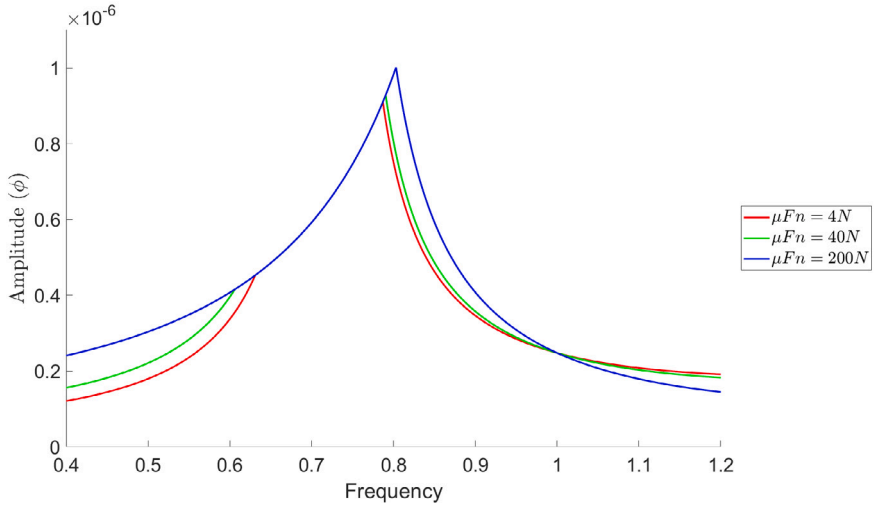

(c) $k_F = 10^6\ N\ m/rad,\ k_N = 10^6\ N\ m/rad$

Fig. 12. Variation of the dynamics/frequency response of the clamp-beam system based on the maximum friction force μF_N and the contact stiffnesses k_F and k_N under the same and constant excitation amplitude.

7. Conclusions

This study proposes a new analytical approach to the problem of frictionally clamped beams forced in bending motion. Cantilever and dual cantilever beam configurations are considered within the scope. The former configuration is a very common model for structures like turbine or compressor blades, whilst the latter configuration essentially represents the dual cantilever fixture configuration of a standard DMA test setup. The friction is modelled using the Jenkins displacement-dependent approach. The system is solved analytically, assuming two distinct regimes of full-stick and full-slip, considering only the first bending mode of the beam. For comparison, a dual cantilever DMA fixture with an epoxy beam sample is taken as a numerical example, and that system is solved with both the derived analytical method and a well-known numerical method that includes finite element method combined with time-marching and frequency sweep without assuming any sort of distinct regimes, providing a thorough and diverse comparison for the proposed new analytical approach.

The results reveal that the system can slip around the resonance. The restrictive friction forces cannot overcome the load transferred to the clamps from the beam around the resonance frequency, which initiates slip. Frictional damping occurs due to the slip, and therefore, the amplitudes of the vibration cannot rise like in a linear model. The parametric study also illustrates that the relation between the parameters and the response of the clamp-beam system is quite complicated due to the nonlinear nature of the system under investigation.

A significant achievement of this study is that the analytical results, obtained from the proposed new method, show good agreement with the numerical model. This concurrence not only validates this new analytical approach but also demonstrates its effectiveness in accurately predicting the complex behaviour of frictionally clamped beams. This could have far-reaching implications for future studies in this field.

Declaration of competing interest

The authors declare that they have no known competing financial interests or personal relationships that could have appeared to influence the work reported in this paper.

Data availability

No data was used for the research described in the article.

Acknowledgements

Mertol Tüfekci would like to acknowledge the support of the Scientific and Technological Research Council of Turkey (TÜBİTAK) (fund BİDEB 2213 2016/2) that makes this research possible.

The authors would also like to acknowledge computational resources and support provided by the Imperial College Research Computing Service (https://doi.org/10.14469/hpc/2232).

References

[1] K. Senthil Kumar, I. Siva, P. Jeyaraj, J.T. Winowlin Jappes, S.C. Amico, N. Rajini, Synergy of fiber length and content on free vibration and damping behavior of natural fiber reinforced polyester composite beams, Mater. Des. 56 (2014) 379–386, https://doi.org/10.1016/j.matdes.2013.11.039.

[2] M. Jočković, G. Radenković, M. Nefovska-Danilović, M. Baitsch, Free vibration analysis of spatial Bernoulli–Euler and Rayleigh curved beams using isogeometric approach, Appl. Math. Model. 71 (2019) 152–172, https://doi.org/10.1016/j.apm.2019.02.002.

[3] U. Eroglu, E. Tufekci, Small-amplitude free vibrations of straight beams subjected to large displacements and rotation, Appl. Math. Model. 53 (2018) 223–241, https://doi.org/10.1016/j.apm.2017.08.028.

[4] H. Koc, E. Tufekci, A novel approach of bending behavior of carbon nanotubes by combining the effects of higher-order boundary conditions and coupling through doublet mechanics, Mech. Adv. Mat. Struct. (2023), https://doi.org/10.1080/15376494.2023.2263767.

[5] E. Tufekci, Exact solution of free in-plane vibration of shallow circular arches, Int. J. Struct. Stab. Dyn. 01 (2001) 409–428, https://doi.org/10.1142/s0219455401000226.

[6] Y.S. Li, T. Xiao, Free vibration of the one-dimensional piezoelectric quasicrystal microbeams based on modified couple stress theory, Appl. Math. Model. 96 (2021) 733–750, https://doi.org/10.1016/j.apm.2021.03.028.

[7] H. Liu, Q. Zhang, Nonlinear dynamics of two-directional functionally graded microbeam with geometrical imperfection using unified shear deformable beam theory, Appl. Math. Model. 98 (2021) 783–800, https://doi.org/10.1016/j.apm.2021.05.029.

[8] P. Foraboschi, S. Schnabl, M. Saje, G. Turk, I. Planinc, Analytical solution of two-layer beam taking into account nonlinear interlayer slip, J. Eng. Mech. 135 (2009) 1129–1146, https://doi.org/10.1061/(asce)em.1943-7889.0000043.

[9] B. Temel, F.F. Çalim, N. Tütüncü, Quasi-static and dynamic response of viscoelastic helical rods, J. Sound Vib. 271 (2004) 921–935, https://doi.org/10.1016/S0022-460X(03)00760-0.

[10] T. Kim, A.M. Hansen, K. Branner, Development of an anisotropic beam finite element for composite wind turbine blades in multibody system, Renew. Energy 59 (2013) 172–183, https://doi.org/10.1016/j.renene.2013.03.033.

[11] B. Akgöz, Ömer Civalek, Vibrational characteristics of embedded microbeams lying on a two-parameter elastic foundation in thermal environment, Composites, Part B, Eng. 150 (2018) 68–77, https://doi.org/10.1016/j.compositesb.2018.05.049.

[12] H.M. Numanoğlu, H. Ersoy, B. Akgöz, Ömer Civalek, A new eigenvalue problem solver for thermo-mechanical vibration of Timoshenko nanobeams by an innovative nonlocal finite element method, Math. Methods Appl. Sci. 45 (2022) 2592–2614, https://doi.org/10.1002/mma.7942.

[13] T.P. Vo, H.T. Thai, M. Aydogdu, Free vibration of axially loaded composite beams using a four-unknown shear and normal deformation theory, Compos. Struct. 178 (2017) 406–414, https://doi.org/10.1016/j.compstruct.2017.07.022.
[14] D.H. Hodges, A.R. Atilgan, M.V. Fulton, L.W. Rehfield, Free-vibration analysis of composite beams, J. Am. Helicopter Soc. 36 (1991) 36–47, https://doi.org/10.4050/JAHS.36.36.
[15] D.A. Saravanos, C.C. Chamis, Integrated mechanics for the passive damping of polymer-matrix composites and composite structures, ASME J. Appl. Mech. 61 (1991) 375–383, https://doi.org/10.1016/0010-4361(91)90379-U, http://ntrs.nasa.gov/search.jsp?R=19910022867.
[16] D.A. Saravanos, C.C. Chamis, Computational simulation of damping in composite structures, J. Reinf. Plast. Compos. 10 (1991) 256–278, https://doi.org/10.1177/073168449101000302.
[17] M.I. Mustafa, Laminated Timoshenko beams with viscoelastic damping, J. Math. Anal. Appl. 466 (2018) 619–641, https://doi.org/10.1016/j.jmaa.2018.06.016.
[18] Şeref D. Albas, H. Ersoy, B. Akgöz, Ömer Civalek, Dynamic analysis of a fiber-reinforced composite beam under a moving load by the Ritz method, Mathematics 9 (2021), https://doi.org/10.3390/math9091048.
[19] Çiğdem Demir, Ömer Civalek, On the analysis of microbeams, Int. J. Eng. Sci. 121 (2017) 14–33, https://doi.org/10.1016/j.ijengsci.2017.08.016.
[20] X. Liu, T. Wada, A. Suzuki, N. Takata, M. Kobashi, M. Kato, Understanding and suppressing shear band formation in strut-based lattice structures manufactured by laser powder bed fusion, Mater. Des. 199 (2021) 109416, https://doi.org/10.1016/j.matdes.2020.109416.
[21] Ömer Civalek, B. Uzun, M. Özgür Yaylı, An effective analytical method for buckling solutions of a restrained fgm nonlocal beam, Comput. Appl. Math. 41 (2022), https://doi.org/10.1007/s40314-022-01761-1.
[22] B. Akgöz, Ömer Civalek, Buckling analysis of functionally graded tapered microbeams via Rayleigh–Ritz method, Mathematics 10 (2022), https://doi.org/10.3390/math10234429.
[23] J.W.S. Rayleigh, The Theory of Sound, vol. 34, second edi ed., Dover Publications, New York, 1945, http://eprints.utas.edu.au/4774/, arXiv:1011.1669v3.
[24] M. Martinez-Agirre, M.J. Elejabarrieta, Dynamic characterization of high damping viscoelastic materials from vibration test data, J. Sound Vib. 330 (2011) 3930–3943, https://doi.org/10.1016/j.jsv.2011.03.025.
[25] P. Franchetti, C. Modena, M.Q. Feng, Nonlinear damping identification in precast prestressed reinforced concrete beams, Comput.-Aided Civ. Infrastruct. Eng. 24 (2009) 577–592, https://doi.org/10.1111/j.1467-8667.2009.00612.x.
[26] S. Adhikari, Damping models for structural vibration, Ph.D. thesis, University of Cambridge, Trinity College, 2000, https://doi.org/10.1006/jsvi.1998.1709, http://engweb.swan.ac.uk/~adhikaris/fulltext/other/ftphd.pdf.
[27] S.H. Crandall, The role of damping in vibration theory, J. Sound Vib. 11 (1970) 3–18, https://doi.org/10.1016/S0022-460X(70)80105-5.
[28] G. Kergourlay, E. Balmès, G. Legal, A characterization of frequency-temperature-prestress effects in viscoelastic films, J. Sound Vib. 297 (2006) 391–407, https://doi.org/10.1016/j.jsv.2006.04.003.
[29] P.J. Torvik, R.L. Bagley, On the appearance of the fractional derivative in the behavior of real materials, J. Appl. Mech. 51 (1984) 294–298, https://doi.org/10.1115/1.3167615.
[30] A. Schmidt, L. Gaul, Finite element formulation of viscoelastic constitutive equations using fractional derivatives, Nonlinear Dyn. 29 (2002) 37–55, https://doi.org/10.1023/A:1016552503411.
[31] H.H. Law, P.L. Rossiter, L.L. Koss, G.P. Simon, Mechanisms in damping of mechanical vibration by piezoelectric ceramic-polymer composite materials, J. Mater. Sci. 30 (1995) 2648–2655, https://doi.org/10.1007/BF00362148.
[32] B. Tang, M.J. Brennan, A comparison of the effects of nonlinear damping on the free vibration of a single-degree-of-freedom system, J. Vib. Acoust. 134 (2012) 1–5, https://doi.org/10.1115/1.4005010, http://vibrationacoustics.asmedigitalcollection.asme.org/article.aspx?articleid=1471676.
[33] B. Tang, M.J. Brennan, A comparison of two nonlinear damping mechanisms in a vibration isolator, J. Sound Vib. 332 (2013) 510–520, https://doi.org/10.1016/j.jsv.2012.09.010.
[34] H.T. Banks, D.J. Inman, On damping mechanisms in beams, J. Appl. Mech., Trans. ASME 58 (1989) 716–723, https://doi.org/10.1115/1.2897253.
[35] B.N. Mcpherson, C. Florida, J.L. Kauffman, C. Florida, Investigation of viscous damping terms for a Timoshenko beam, in: AIAA/ASCE/AHS/ASC Structures, Structural Dynamics, and Materials Conference, January 2018, pp. 1–12, https://doi.org/10.2514/6.2018-0456.
[36] Y. Lei, T. Murmu, S. Adhikari, M.I. Friswell, Dynamic characteristics of damped viscoelastic nonlocal Euler-Bernoulli beams, Eur. J. Mech. A, Solids 42 (2013) 125–136, https://doi.org/10.1016/j.euromechsol.2013.04.006.
[37] F. Fontanela, A. Grolet, L. Salles, A. Chabchoub, A.R. Champneys, S. Patsias, N. Hoffmann, Dissipative solitons in forced cyclic and symmetric structures, in: Mechanical Systems and Signal Processing, 2018, pp. 3–5, http://arxiv.org/abs/1804.01321, arXiv:1804.01321.
[38] F. Fontanela, A. Grolet, L. Salles, N. Hoffmann, Computation of quasi-periodic localised vibrations in nonlinear cyclic and symmetric structures using harmonic balance methods, J. Sound Vib. (2019), https://doi.org/10.1016/j.jsv.2018.09.002.
[39] A.G. Egorov, A.M. Kamalutdinov, A.N. Nuriev, Evaluation of aerodynamic forces acting on oscillating cantilever beams based on the study of the damped flexural vibration of aluminium test samples, J. Sound Vib. 421 (2018) 334–347, https://doi.org/10.1016/j.jsv.2018.02.006.
[40] J. Filipiak, L. Solarz, K. Zubko, Analysis of damping effect on beam vibration, Mol. Quantum Acoust. 27 (2006) 79–88, http://mqa.ogpta.polsl.pl/files-articles/27/pdf/079-088%7B%5C_%7DFilipiak%7B%5C_%7DSolarz%7B%5C_%7DZubko.pdf.
[41] S. Schmid, C. Hierold, Damping mechanisms of single-clamped and prestressed double-clamped resonant polymer microbeams, J. Appl. Phys. 104 (2008), https://doi.org/10.1063/1.3008032.
[42] M. Malikan, V.B. Nguyen, F. Tornabene, Damped forced vibration analysis of single-walled carbon nanotubes resting on viscoelastic foundation in thermal environment using nonlocal strain gradient theory, Int. J. Eng. Sci. Technol. (2018), https://doi.org/10.1016/j.jestch.2018.06.001.
[43] G.Y. Zhang, X.L. Gao, Z.Y. Guo, A non-classical model for an orthotropic Kirchhoff plate embedded in a viscoelastic medium, Acta Mech. 228 (2017) 3811–3825, https://doi.org/10.1007/s00707-017-1906-4.
[44] S.W. Shaw, On the dynamic response of a system with dry friction, J. Sound Vib. 108 (1986) 305–325, https://doi.org/10.1016/S0022-460X(86)80058-X.
[45] B. He, H. Ouyang, S. He, X. Ren, Stick-slip vibration of a friction damper for energy dissipation, Adv. Mech. Eng. 9 (2017) 1–13, https://doi.org/10.1177/1687814017713921.
[46] B. Feeny, A. Guran, N. Hinrichs, K. Popp, A historical review on dry friction and stick-slip phenomena, https://doi.org/10.1115/1.3099008, 1998.
[47] P.M. Fishbane, S. Gasiorowicz, S.T. Thornton, Physics for Scientists and Engineers. I, extended e ed., Prentice Hall, Englewood Cliffs, New Jersey, 1993.
[48] M.C. Ferris, F. Tin-Loi, Limit analysis of frictional block assemblies as a mathematical program with complementarity constraints, Int. J. Mech. Sci. 43 (2001) 209–224, https://doi.org/10.1016/S0020-7403(99)00111-3.
[49] Y. Mabuchi, T. Hanazato, M. Watabe, Static shear friction tests on the model marble columns of the Parthenon for the aseismic retrofitting, Trans. Built Environ. 4 (1993) 475–482.
[50] I.N. Psycharis, J.V. Lemos, D.Y. Papastamatiou, C. Zambas, C. Papanponopoulos, Numerical study of the seismic behaviour of a part of the Parthenon Pronaos, Earthq. Eng. Struct. Dyn. 32 (2003) 2063–2084, https://doi.org/10.1002/eqe.315, https://onlinelibrary.wiley.com/doi/abs/10.1002/eqe.315?casa_token=Et9vCVFGlB8AAAAA:oxvg1Cf1nmutjjh_VbRogqCdilIRdjm8nN0UYVLwKQFKaViL0kZ4fph1c2DiUdqeGw7e5SDgapBvL5U, https://onlinelibrary.wiley.com/doi/abs/10.1002/eqe.315?casa%7B%5C_%7Dtoken=Et9vCVFGlB8AAAA.
[51] M. Courtel, M.L. Tichvinski, A brief history of friction, Nav. Eng. J. (June 1964) 451–460, https://doi.org/10.1111/j.1559-3584.1964.tb04759.x.
[52] C.A. Coulomb, Theorie des machines simples, Mem. Math. Phys. Acad. Sci. 10 (1785) 161–331.
[53] E. Pennestrì, V. Rossi, P. Salvini, P.P. Valentini, Review and comparison of dry friction force models, Nonlinear Dyn. 83 (2016) 1785–1801, https://doi.org/10.1007/s11071-015-2485-3.

[54] M. Jean, E. Pratt, A system of rigid bodies with dry friction, https://doi.org/10.1016/0020-7225(85)90060-6, 1985.
[55] J.A.C. Martins, F.M.F. Simões, F. Gastaldi, M.D.P. Monteiro Marques, Dissipative graph solutions for a 2 degree-of-freedom quasistatic frictional contact problem, Int. J. Eng. Sci. 33 (1995) 1959–1986, https://doi.org/10.1016/0020-7225(95)00039-Z.
[56] Z. Skup, Analysis of damping of vibrations through a frictional damper, J. Theor. Appl. Mech. 48 (2010) 465–478.
[57] E.J.E.J. Berger, Friction modeling for dynamic system simulation, Appl. Mech. Rev. 55 (2002) 535, https://doi.org/10.1115/1.1501080.
[58] L. Půst, L. Pešek, A. Radolfová, Various types of dry friction characteristics for vibration damping, Eng. Mech. 18 (2011) 203–224, http://dlib.lib.cas.cz:8080/2749/.
[59] F. Marín, F. Alhama, J.A. Moreno, Modelling of stick-slip behaviour with different hypotheses on friction forces, https://doi.org/10.1016/j.ijengsci.2012.06.002, 2012.
[60] I.R. Ionescu, J.C. Paumier, On the contact problem with slip displacement dependent friction in elastostatics, https://doi.org/10.1016/0020-7225(95)00109-3, 1996.
[61] L. Xu, M.W. Lu, Q. Cao, Nonlinear vibrations of dynamical systems with a general form of piecewise-linear viscous damping by incremental harmonic balance method, Phys. Lett. A 301 (2002) 65–73, https://doi.org/10.1016/S0375-9601(02)00960-X, http://linkinghub.elsevier.com/retrieve/pii/S037596010200960X.
[62] X. Tan, R.J. Rogers, Equivalent viscous damping models of Coulomb friction in multi-degree-of-freedom vibration systems, J. Sound Vib. 185 (1995) 33–50, https://doi.org/10.1006/jsvi.1994.0362.
[63] T. Friis, M. Tarpø, E.I. Katsanos, R. Brincker, Equivalent linear systems of nonlinear systems, J. Sound Vib. 469 (2020), https://doi.org/10.1016/j.jsv.2019.115126.
[64] L.E. Goodman, J.H. Klumpp, Analysis of slip damping with reference of turbine-blade vibration, J. Appl. Mech. 32 (1956) 421–429.
[65] G. Levy, Modelling of Coulomb damping and wear of vibrating systems, Wear 64 (1980) 57–82, https://doi.org/10.1016/0043-1648(80)90094-0.
[66] O.Y. Zharii, An exact solution of a time-dependent frictional contact problem for two elastic spheres, https://doi.org/10.1016/0020-7225(95)00094-1, 1996.
[67] Y. Sun, J. Yuan, L. Pesaresi, L. Salles, Nonlinear vibrational analysis for integrally bladed disk using frictional ring damper, J. Phys. Conf. Ser. 1106 (2018), https://doi.org/10.1088/1742-6596/1106/1/012026.
[68] C. Pierre, A.A. Ferri, E.H. Dowell, Multi-harmonic analysis of dry friction damped systems using an incremental harmonic balance method, J. Appl. Mech. 52 (2009) 958, https://doi.org/10.1115/1.3169175.
[69] H.I. Won, J. Chung, Numerical analysis for the stick-slip vibration of a transversely moving beam in contact with a frictional wall, J. Sound Vib. 419 (2018) 42–62, https://doi.org/10.1016/j.jsv.2017.12.037.
[70] C. Gastaldi, T.M. Berruti, Competitive time marching solution methods for systems with friction-induced nonlinearities, Appl. Sci. (Switzerland) 8 (2018), https://doi.org/10.3390/app8020291.
[71] N.A. Labanda, P. Behnoudfar, V.M. Calo, An explicit predictor/multicorrector time marching with automatic adaptivity for finite-strain elastodynamics, J. Comput. Phys. 472 (2023), https://doi.org/10.1016/j.jcp.2022.111696.
[72] V.N. Burlayenko, T. Sadowski, Nonlinear dynamic analysis of harmonically excited debonded sandwich plates using finite element modelling, Compos. Struct. 108 (2014) 354–366, https://doi.org/10.1016/j.compstruct.2013.09.042.
[73] A. Klarbring, A. Mikelić, M. Shillor, Frictional contact problems with normal compliance, Int. J. Eng. Sci. 26 (1988) 811–832, https://doi.org/10.1016/0020-7225(88)90032-8.
[74] A.A. Ferri, A.C. Bindemann, Damping and vibrations of beams with various types of frictional support conditions, Trans. Am. Soc. Mech. Eng. 114 (1992) 289–296.
[75] G.P. Wright, J.J. O'Connor, Finite-element analysis of alternating axial loading of an elastic plate pressed between two elastic rectangular blocks with finite friction, Int. J. Eng. Sci. 9 (1971) 555–570, https://doi.org/10.1016/0020-7225(71)90038-3.
[76] H. Ramsey, Analysis of interwire friction in multilayered cables under uniform extension and twisting, https://doi.org/10.1016/0020-7403(90)90011-7, 1990.
[77] A. Cicirello, R.S. Langley, The vibro-acoustic analysis of built-up systems using a hybrid method with parametric and non-parametric uncertainties, J. Sound Vib. 332 (2013) 2165–2178, https://doi.org/10.1016/j.jsv.2012.05.040.
[78] A. Cherki, G. Plessis, B. Lallemand, T. Tison, P. Level, Fuzzy behavior of mechanical systems with uncertain boundary conditions, Comput. Methods Appl. Mech. Eng. 189 (2000) 863–873, https://doi.org/10.1016/S0045-7825(99)00401-6.
[79] L. Frýba, S. Nakagiri, N. Yoshikawa, Stochastic finite elements for a beam on a random foundation with uncertain damping under a moving force, https://doi.org/10.1006/jsvi.1993.1146, 1993.
[80] T.G. Ritto, R. Sampaio, E. Cataldo, Timoshenko beam with uncertainty on the boundary conditions, J. Braz. Soc. Mech. Sci. Eng. 30 (2009) 295–303, https://doi.org/10.1590/s1678-58782008000400005.
[81] S. Li, E. Reynders, K. Maes, G. De Roeck, Vibration-based estimation of axial force for a beam member with uncertain boundary conditions, J. Sound Vib. 332 (2013) 795–806, https://doi.org/10.1016/j.jsv.2012.10.019.
[82] H. Ahmadian, H. Jalali, F. Pourahmadian, Nonlinear model identification of a frictional contact support, Mech. Syst. Signal Process. 24 (2010) 2844–2854, https://doi.org/10.1016/j.ymssp.2010.06.007.
[83] K. Asadi, H. Ahmadian, H. Jalali, Micro/macro-slip damping in beams with frictional contact interface, J. Sound Vib. 331 (2012) 4704–4712, https://doi.org/10.1016/j.jsv.2012.05.026.
[84] E. Ciğeroğlu, H.N. Özgüven, Nonlinear vibration analysis of bladed disks with dry friction dampers, J. Sound Vib. 295 (2006) 1028–1043, https://doi.org/10.1016/j.jsv.2006.02.009.
[85] L. Marino, A. Cicirello, Dynamic response of multi-degree-of-freedom systems with a Coulomb friction contact under harmonic excitation, Nonlinear Dyn. 106 (2021) 1675–1709, https://doi.org/10.1007/s11071-021-06966-3.